THE JOURNAL OF PHYSICAL CHEMISTRY Letters

Letter

pubs.acs.org/JPCL

Influence of Solvent Relaxation on Ultrafast Excited-State Proton Transfer to Solvent

Tatu Kumpulainen,* Arnulf Rosspeintner, Bogdan Dereka, and Eric Vauthey*

Department of Physical Chemistry, University of Geneva, 30 Quai Ernest Ansermet, Geneva, Switzerland

Supporting Information

ABSTRACT: A thorough understanding of the microscopic mechanism of excited-state proton transfer (ESPT) and the influence of the solvent environment on its dynamics are of great fundamental interest. We present here a detailed investigation of an ESPT to solvent (DMSO) using time-resolved broadband fluorescence and transient absorption spectroscopies. All excited-state species are resolved spectrally and kinetically using a global target analysis based on the two-step Eigen-Weller model. Reversibility of the initial short-range proton transfer producing excited contact ion pairs (CIP*) is observed unambiguously in fluorescence and must be explicitly considered to obtain the individual rate constants. Close inspection of the early dynamics suggests that the relative populations of the protonated form (ROH*) and CIP* are governed by solvent relaxation that influences the relative energies of the excited states. This constitutes a breakdown of the Eigen-Weller model, although the overall agreement between the data and the analysis using classical rate equations is excellent.

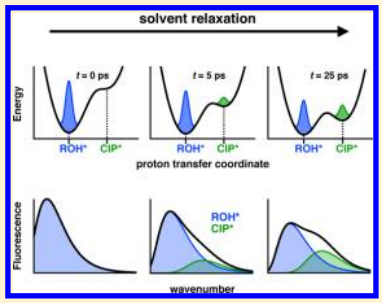

Photoinduced proton transfer plays a key role in many chemical and biological processes.[1] Therefore, it continues to draw the attention of a broad scientific community, as demonstrated by a recent special issue on this very topic.[2] Despite the wealth of investigations on excited-state proton-transfer (ESPT) reactions,[3−6] several fundamental aspects are still under discussion. For example, the influence of the solvent environment on ESPT is recognized from both experimental[7,8] and theoretical[9−11] viewpoints but only a few studies have explicitly accounted for solvent relaxation and its influence on the ESPT.[12−15] There is, however, some experimental evidence that suggests that the initial proton-transfer step of strong photoacids is controlled by solvent relaxation.[13,14] Second, ESPT reactions are usually modeled according to the Eigen-Weller model (Scheme 1), which consists of an initial short-range proton-transfer producing contact ion pairs, followed by a diffusion-controlled separation into free anions.[16,17] However, this model is often discussed only qualitatively, and detailed investigations resolving all individual rate constants and relaxation pathways are scarce. Few studies have demonstrated that the ESPT dynamics of several photoacids are consistent with the Eigen-Weller model, but the contact ion pairs were suggested to be spectrally indistinguishable from the free anions.[12,14,18−20] Hence studies resolving all excited-state species both kinetically and spectrally are still missing. Lastly, data obtained using different spectroscopic techniques have sometimes resulted in differing interpretations of the same process. This is best demonstrated by studies on 8-hydroxypyrene-1,3,6-trisulfonate (**HPTS**). Its deprotonation kinetics in water are governed by three time constants of ∼300 fs, ∼3 ps, and ∼90 ps, where the fastest and the slowest time constants are attributed to solvent relaxation around the locally excited state and dissociation of the ion pair, respectively. The intermediate step, however, remains controversial and has been suggested to originate from hydrogen-bond rearrangement,[21] LE-CT transition,[22−25] solvation dynamics,[26] or formation of the intermediate contact ion pairs[12,18,27] depending on the study. No unambiguous evidence of one or the other interpretation has been provided, and the debate continues to date.[25,27]

The aim of the current work is to address the above-discussed issues on ESPT to solvent. This is achieved by measuring the ESPT dynamics of a 1,8-naphthalimide photoacid, **SHONI**, in dimethyl sulfoxide (DMSO). This compound exhibits a ground-state pK_a of 8, which decreases to −2 in the excited state. The strong photoacidity can be attributed to an intramolecular charge transfer (ICT) from the hydroxyl oxygen to the aromatic imide group upon $S_1 \leftarrow S_0$ excitation. The

Scheme 1. Two-Step Eigen-Weller Model for Excited-State Proton Transfer to Solvent[a]

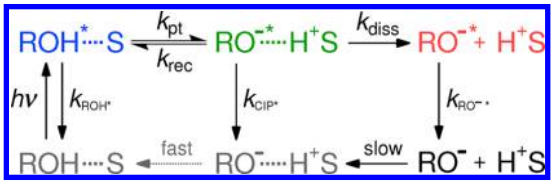

[a]The first step consists of a reversible short-range proton transfer from the protonated form (ROH*) to solvent (S) producing contact ion pairs (CIP*), followed by a full dissociation into free anions (RO^-*). All relevant rate constants are indicated in the Scheme.

Received: July 27, 2017
Accepted: September 5, 2017
Published: September 5, 2017

DOI: 10.1021/acs.jpclett.7b01956
J. Phys. Chem. Lett. 2017, 8, 4516−4521

ESPT dynamics in DMSO have been investigated before using a single-wavelength picosecond time-correlated single photon counting, but the short time-scale dynamics are fully unexplored.[28] We present now a detailed investigation on the ultrafast ESPT dynamics of **SHONI** using three femtosecond (fs) broadband techniques: visible and mid-IR transient absorptions (visTA and mid-IRTA), in addition to fluorescence up-conversion (FLUPS).[29] The data are analyzed using a global target analysis according to Scheme 1. In the case of the FLUPS data, solvent relaxation is explicitly accounted for by using a recently developed global analysis in which each fluorescent species is represented by a time-dependent band-shape (log-normal) function.[30,31] The solvent relaxation and relative populations are independently accessed from the band positions and the band integrals, respectively. The experimental and data analysis methods are described in detail in the Supporting Information. Combination of these techniques together with the global target analysis yields much deeper insight into the mechanism and dynamics of ESPT to solvent and allows us to demonstrate the key factors that are required for a full kinetic and spectral characterization of all excited-state species. Moreover, it enables the recovery of the true species spectra as well as all the individual rate constants and facilitates a detailed investigation of the influence of solvent relaxation on the population dynamics.

The UV−vis absorption spectra of the protonated (ROH) and deprotonated (RO^-) forms of **SHONI**(Chart 1) in DMSO

Chart 1. Structures of the Protonated (ROH, blue) and Deprotonated (RO^-, red) Forms of the Photoacid SHONI

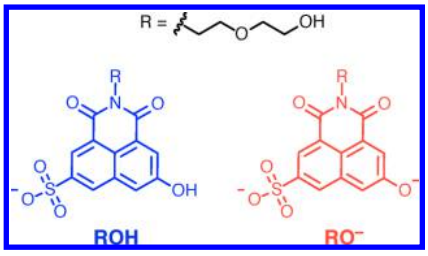

and water are shown in Figure 1A. The $S_1 \leftarrow S_0$ band maxima of the ROH form are nearly identical in DMSO (389 nm) and water (384 nm). The emission spectra upon excitation of ROH in both solvents exhibit a relatively weak band at ∼400−500 nm attributed to ROH* and a much stronger band at ∼550−800 nm originating from RO^-*.[28] Interestingly, the absorption band of the deprotonated form in DMSO (511 nm) is drastically red-shifted by nearly 3000 cm^{-1} compared with water (444 nm). The emission peak maxima, on the contrary, appear at similar wavelengths in both solvents (638 nm in DMSO, 664 nm in water, $\Delta\tilde{\nu}$ = 630 cm^{-1}). This is attributed to differences in hydrogen-bond-donating ability of the solvents. Water is able to donate hydrogen bonds that significantly stabilize the ground-state anion with a formal negative charge on the deprotonated hydroxyl oxygen. This hydrogen bond is cleaved in the excited state, resulting in destabilization of the ground state compared with the hydrogen-bonded anion.[8] Similarly, a cleavage of the hydrogen bond between a deprotonated oxygen and a protonated solvent molecule, that is, full dissociation of contact ion pairs (CIP*) into free anions (RO^-*), results in a significant red shift of the fluorescence facilitating spectral separation of the two species.

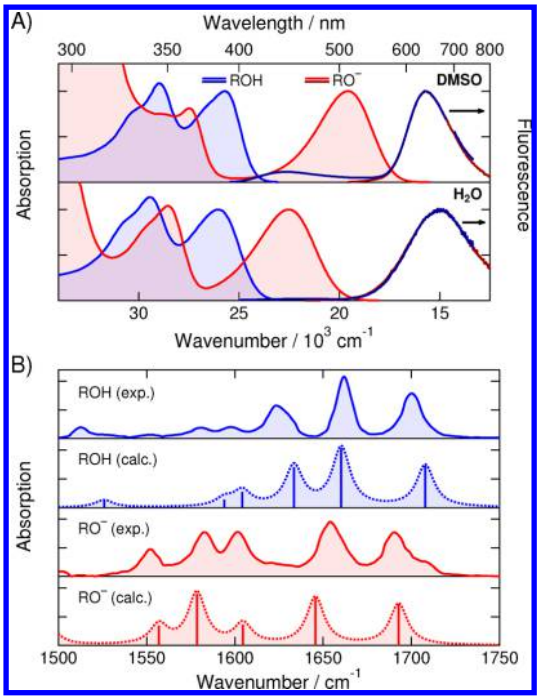

Figure 1. (A) UV−vis absorption (solid lines with fill) and emission (solid lines) spectra of the protonated (ROH, blue) and deprotonated (RO^-, red) forms of **SHONI** in DMSO (top) and water (bottom). (All spectra are presented against wavenumbers, but the wavelength scale is shown on the top axis for comparison.) (B) Measured (solid lines) and calculated (DFT: PBE0/6-311+G(d,p), dashed lines) mid-IR absorption spectra of the protonated (ROH, blue) and deprotonated (RO^-, red) forms of **SHONI** in DMSO. The calculated frequencies have been scaled by 0.968, and the stick spectra are broadened by using Lorentzian line shape functions for a visual comparison.

The IR absorption spectra of the ROH and RO^- forms in DMSO are shown in Figure 1B. The frequencies and corresponding normal modes are summarized in Table S1. The three main absorption bands of the ROH form are attributed to the symmetric (1700 cm^{-1}) and antisymmetric (1662 cm^{-1}) C═O stretch and aromatic ring vibrations (1624 cm^{-1}). Additional weaker transitions are observed at lower frequencies that originate mostly from aromatic ring vibrations of the 1,8-naphthalimide skeleton. Upon deprotonation, all peaks red shift, and the low-frequency modes gain intensity in agreement with the DFT calculations. The changes are attributed to increased electron density on both the aromatic system and on the imide carbonyl groups due to the deprotonation.[32,33] The red shifts of these vibrations therefore report on the magnitude of the ICT from the hydroxyl substituent to the aromatic system and are used to probe the ESPT process in the mid-IRTA experiments.

Time-resolved spectra were measured in slightly acidified DMSO (λ_{exc} = 400 nm). All data are summarized in Figure 2, which shows time-resolved spectra (left), time traces together with the best fits (middle), and the species associated (difference) spectra (right) obtained from the target analysis according to Scheme 1. (See the Supporting Information for details and 3D-surface plots of the full data sets, fits, and residuals.) Each data set could also be adequately fitted with three global lifetimes with time constants of ∼6 ps, ∼500 ps, and ∼16 ns corresponding to a sequential model with three observable species (A → B → C →; see Section 4.4 of the

DOI: 10.1021/acs.jpclett.7b01956
J. Phys. Chem. Lett. 2017, 8, 4516−4521

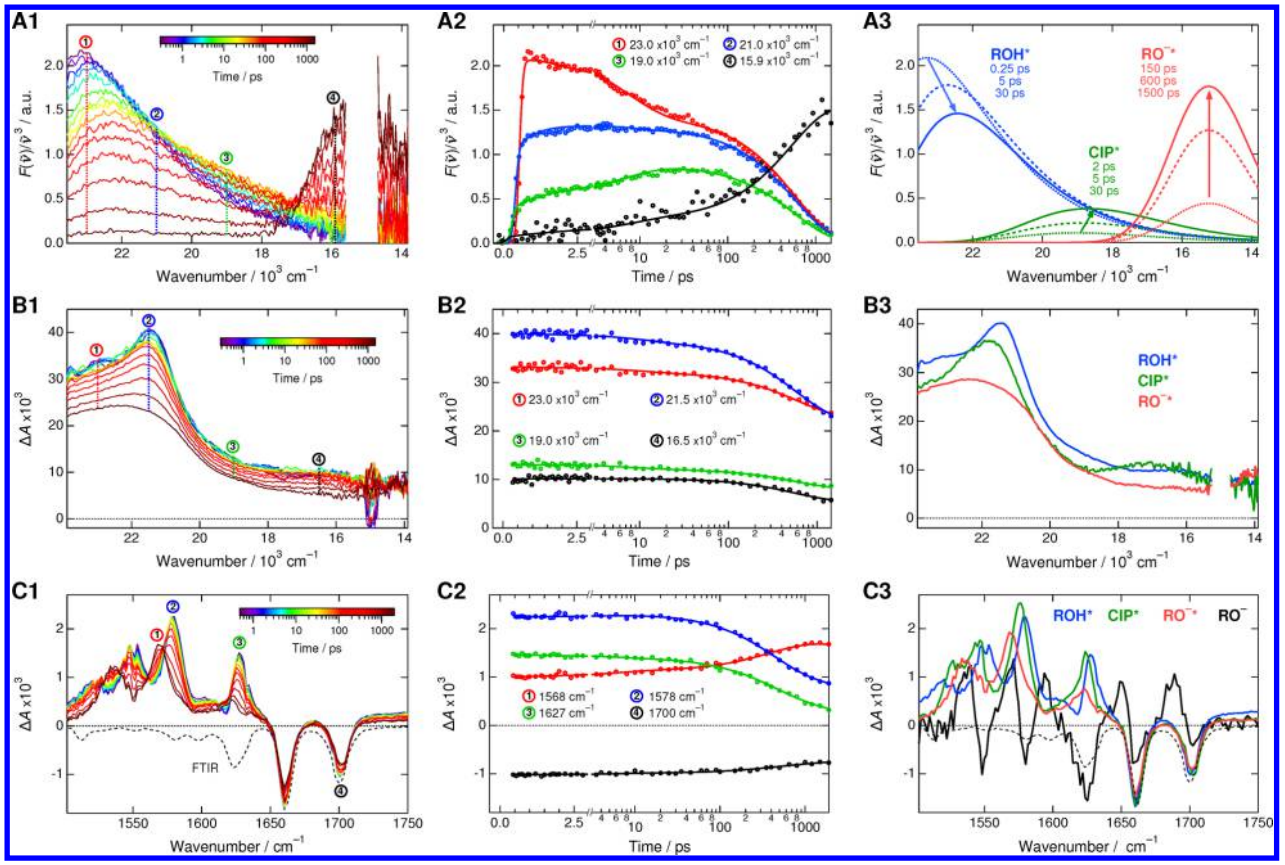

Figure 2. Summary of the time-resolved data of **SHONI** in slightly acidified DMSO showing representative spectra (left), time traces together with the best fits (middle), and species associated (difference) spectra (right) obtained from the target analysis according to Scheme 1. Excitation was at 400 nm in all experiments. The FLUPS data (A) were analyzed using a global model where each of the species is modeled as a log-normal band-shape function allowed to undergo dynamic Stokes shift, whereas the visTA (B) and mid-IRTA (C) data were analyzed assuming static species associated difference spectra. Stimulated emission was subtracted from the original visTA data (Figure S3). Inverted and scaled stationary IR-spectrum of ROH in DMSO is indicated in C1 and C3 by the dashed line. The ground-state anion was observed only in the mid-IRTA experiment.

Supporting Information for a detailed comparison between the two models). We will first describe each data set separately before discussing the main findings of the study.

Broadband fluorescence spectra (Figure 2A1) show that the ROH* emission is initially at 23×10^3 cm^{-1} and then red shifts by ca. 1000 cm^{-1} and decays partially during the first 10−30 ps. This partial decay is accompanied by a concomitant rise of a broad intermediate emission around 19×10^3 cm^{-1}, which is attributed to CIP*. At this point, the spectrum clearly consists of two emissive species and cannot be represented by a single band-shape function. Afterward, ROH* and CIP* decay synchronously, and a new band around 15×10^3 cm^{-1} rises that can be ascribed to RO$^-$*, in agreement with the steady-state spectrum. The dynamic frequency shift of the ROH* and CIP* fluorescence bands was modeled with a biexponential function, and the resulting average solvent relaxation time is $\langle\tau_{solv}\rangle \approx 5$ ps. Because the RO$^-$* emission appears on a much longer time scale, its peak frequency remains constant. The biexponential decay of the ROH* population reveals that the first step is reversible and results in an equilibrium between ROH* and CIP*, which then undergoes a full dissociation into RO$^-$*.

The original visTA spectra consist of positive and negative signals due to excited-state absorption (ESA) and stimulated emission (SE), respectively. To evaluate changes in the pure ESA spectra, we subtracted the SE from the original visTA data (Figure S3). The ESA spectra (Figure 2B1) show a broad absorption band at 21.5×10^3 cm^{-1}, which decays and slightly shifts on a long time scale. Surprisingly, hardly any spectral changes are observed during the establishment of the equilibrium between ROH* and CIP*. The resulting species associated difference spectra (SADS) of ROH* and CIP* are similar (Figure 2B3), but the main reason for the lack of changes is the relatively low equilibrium population of CIP*. The similarity of the SADS indicates that the excited-state potential energy surfaces of these two species are very similar. Hence, identification of the intermediate CIP* based on the ESA spectra is not really feasible. Clear changes are, however, observed in the stimulated emission (Figure S6), as already demonstrated by the time-resolved emission spectra (FLUPS).

The mid-IRTA spectra (Figure 2C1) exhibit red shifts of all absorption bands upon excitation. This is ascribed to the ICT character of the excited state, which increases the electron density on the imide carbonyls and the aromatic system. The three main bands originating from the aromatic, antisymmetric, and symmetric C═O stretch vibrations shift initially by ca. 70−80 cm^{-1} and exhibit only modest changes during the equilibration. The SADS of ROH* and CIP* are, however, different and demonstrate further enhancement of the ICT character upon the formation of CIP*. Similar to visTA, the absence of spectral changes during the first 10−30 ps can be attributed to the low CIP* population. All bands exhibit further red shifts upon full dissociation into RO$^-$*, where the negative charge of the deprotonated hydroxyl oxygen is fully delocalized

DOI: 10.1021/acs.jpclett.7b01956
J. Phys. Chem. Lett. 2017, 8, 4516−4521

Table 1. Summary of the Kinetic Parameters Obtained from the Global Target Analyses of the Broadband Data[a]

$k_{pt}/10^{10}$ s^{-1}	$k_{rec}/10^{10}$ s^{-1}	$k_{diss}/10^{9}$ s^{-1}	$k_{ROH*}/10^{8}$ s^{-1}[b]	$k_{CIP*}/10^{7}$ s^{-1}[c]	$k_{RO^-*}/10^{7}$ s^{-1}
4.8 ± 1.1	10 ± 3	5.5 ± 1.0	2.9 ± 0.5	6.3 ± 0.4	6.3 ± 0.4
(21 ± 5 ps)$^{-1}$	(10 ± 4 ps)$^{-1}$	(180 ± 30 ps)$^{-1}$	(3.4 ± 0.5 ns)$^{-1}$	(16 ± 1 ns)$^{-1}$	(16 ± 1 ns)$^{-1}$

[a]Values represent the average values obtained from the analyses of the three data sets and errors are the corresponding standard deviations. [b]Direct decay of ROH* was adjusted to obtain a constant ground-state bleach of the different species in the mid-IRTA experiment at ~1700 cm^{-1}. [c]Direct decay of CIP* was set equal to the decay of RO$^-$* ($k_B = k_C$); see the Supporting Information for full details of the fitting procedures and boundary conditions used.

on the aromatic system. These marker bands reliably report on the magnitude of the ICT and allow for monitoring of the ESPT process. Finally, a small population of the ground-state anions, RO$^-$, is resolved as the last species that does not decay during the experimental time window. In RO$^-$, the negative charge is mostly localized on the hydroxyl oxygen, and the ground-state bleach of ROH largely overlaps with the induced absorption of RO$^-$.

The rate constants obtained from the target analysis according to Scheme 1 are summarized in Table 1, and the relative concentrations of each species are presented in Figure 4A. The rate of the partial decay of ROH*, that is, establishment of the equilibrium, is related to the sum of the forward and backward rates, $\tau_1^{ROH*} \approx 1/(k_{pt} + k_{rec}) = 6.8$ ps, and is close to $\langle\tau_{solv}\rangle \approx 5$ ps. To get a more detailed picture of the early kinetics, we extracted the pure CIP* emission spectra shown in Figure 3A (see the Supporting Information for details) and fitted the rise with a three-exponential function (Figure 3B). The rise is clearly multiexponential with an average time constant of $\langle\tau_{rise}\rangle = 6.1$ ps, and the individual time constants are comparable to typical solvation times in DMSO, as observed with standard solvation probes.[31,34] This strongly suggests that the establishment of the equilibrium is

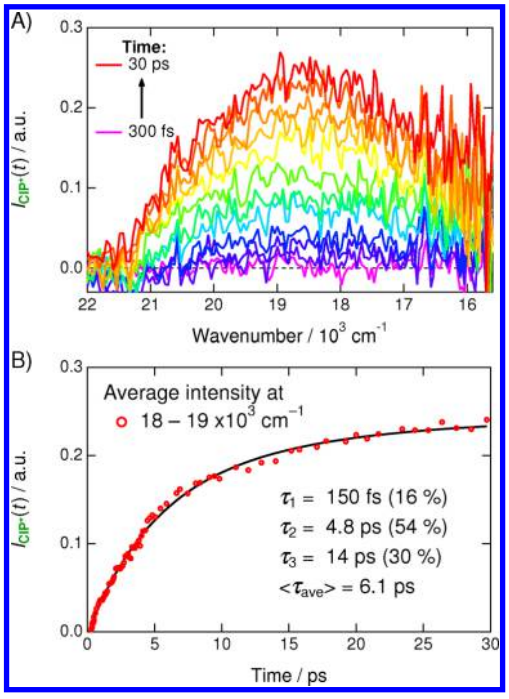

Figure 3. (A) Pure emission spectra of CIP* extracted from the total time-resolved fluorescence as described in the Supporting Information. (B) Average CIP* emission between (18 and 19) × 10^3 cm^{-1} (markers) together with a three-exponential fit of the rise (solid line). The resulting lifetimes (amplitudes) are indicated in the inset.

"solvent-controlled" and the relative population of CIP* increases as a function of the solvent relaxation. Moreover, this would imply that the intrinsic proton transfer rates k_{pt} and k_{rec} are significantly larger than the rate of the solvent relaxation. Hence the absolute magnitudes of k_{pt} and k_{rec} resulting from the target analysis reflect the average solvent relaxation rate, whereas the ratio is related to the relative equilibrium populations of ROH* and CIP*. In this case, $K_{pt} = k_{pt}/k_{rec} \approx 0.5$ ($\Delta G_{pt} \approx 2$ kJ/mol ≈ 180 cm^{-1}) and the equilibrium population of CIP* is 33%. The rate constant for full dissociation (k_{diss}), on the contrary, is equal to a diffusion-limited rate, although the apparent lifetime (~500 ps) is significantly longer due to the relatively low equilibrium population of CIP*. (See the Supporting Information for details.)

The influence of the solvent relaxation is further visualized in the energy level diagram depicted in Figure 4B. The S_0–S_1

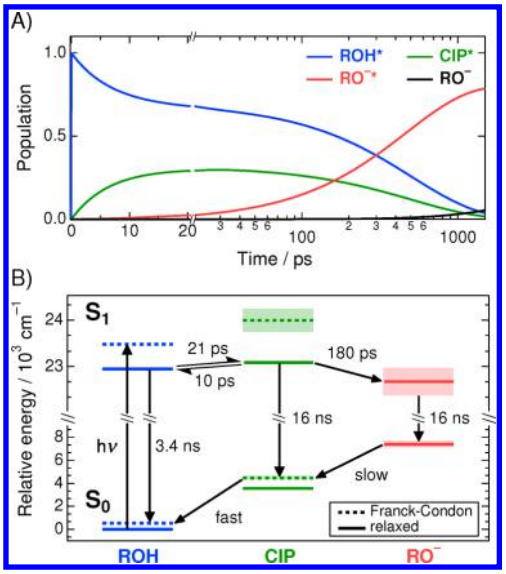

Figure 4. (A) Relative populations of the different species calculated according to Scheme 1 with the rate constants obtained from the target analyses (Table 1). (B) Relative energies of the ground and excited states of the different species. The dashed lines represent the energies before solvent relaxation. The shaded areas indicate the uncertainties in the relative energies.

energy gaps are estimated from the peak frequencies of the emission bands, and the unrelaxed peak positions (before solvent relaxation) are obtained by adding 50% of the total dynamic Stokes shift to the relaxed energy gaps.[35] The energy of the relaxed CIP* relative to the relaxed ROH* is related to the driving force of the reaction and can be calculated from K_{pt}. The energy of RO$^-$ relative to CIP is estimated from the absorption maxima of the ground-state anions measured in water (CIP) and DMSO (RO$^-$) and was set to 3000 ± 300

DOI: 10.1021/acs.jpclett.7b01956
J. Phys. Chem. Lett. 2017, 8, 4516–4521

cm^{-1}. This assumes that the blue shift in water originates solely from the stabilization of the ground-state anion due to hydrogen bonding. The uncertainties in the relative energies are represented by the shaded areas. Upon vertical excitation, the energy of CIP* is significantly higher than that of ROH* and ESPT cannot take place; however, because CIP* has stronger ICT character, as demonstrated by the mid-IRTA experiments, it experiences larger solvent stabilization and the energy gap is reduced during solvent relaxation. The similarity of the time scales for the solvation and rise of the CIP* emission suggests that, at any given time, the relative populations of ROH* and CIP* are in quasi-equilibrium governed by the relative positions of the excited-state energies. Full dissociation into RO^-*, on the contrary, is controlled by diffusion, as demonstrated by the agreement with the calculated diffusion-limited rate constant. Because of our limited time window (1.5 ns) we are not able to assess the reversibility of the dissociation process, although the relative energies suggest that the reverse reaction is energetically unfavorable. In addition, the relative energies demonstrate that red shift of the fluorescence upon deprotonation originates from differences in the ground-state rather than in the excited-state energies.

In conclusion, a full spectral and kinetic characterization of the species involved in ESPT to solvent is not a trivial task. The intermediate CIP* is best observed in the fluorescence (both spontaneous and stimulated) due to its blue-shifted emission relative to that of RO^-*.[36−38] This should be a general phenomenon in cases where the stationary absorption spectrum of the deprotonated form is blue-shifted in protic solvents compared with aprotic solvents of similar polarities. The observed spectrum of CIP* is, however, broad and largely overlaps with the spectra of ROH* and RO^-*, complicating the analysis using a single-wavelength detection. Solvent relaxation further contributes to the nonexponentiality of the single-wavelength decays. These complications are largely avoided in the global analysis based on the time-dependent band-shape functions. The reversibility of the initial step is manifested as a biphasic decay of the ROH* population. Detailed analysis of the early kinetics, however, reveals that the establishment of the final equilibrium is multiexponential and follows the solvent relaxation, although the Eigen-Weller model provides an excellent approximation of the overall behavior. The transient absorption spectra (both visible and mid-IR) show only modest changes during the establishment of the equilibrium, which can be ascribed to the low equilibrium population of CIP* and, second, to the similarity between the species associated spectra of ROH* and CIP*. Solvent relaxation is not seen unambiguously in the TA spectra but is intermixed with the initial proton-transfer step. Therefore, discrimination between the species and hence between different photochemical models is nearly impossible without a detailed knowledge of the true species spectra.

■ ASSOCIATED CONTENT

Supporting Information

The Supporting Information is available free of charge on the ACS Publications website at DOI: 10.1021/acs.jpclett.7b01956.

Experimental and computational details, frequencies and corresponding normal modes of the mid-IR spectra, experimental setups and data analysis methods for time-resolved experiments, additional 3D-surface plots of the broadband data, fits and residuals, fitting parameters, and boundary conditions of the target analyses, removal of stimulated emission from visTA data, comparison between the sequential and target models, relation between the apparent lifetimes and rate constants, extracting pure CIP* emission, and estimation of the diffusion-limited separation. (PDF)

■ AUTHOR INFORMATION

Corresponding Authors

*E-mail: tatu.kumpulainen@unige.ch. Tel: +41 (0)22 379 6537. Fax: +41 (0)22 379 6518.
*E-mail: eric.vauthey@unige.ch.

ORCID

Tatu Kumpulainen: 0000-0001-9469-9294
Arnulf Rosspeintner: 0000-0002-1828-5206
Bogdan Dereka: 0000-0003-2895-7915
Eric Vauthey: 0000-0002-9580-9683

Notes

The authors declare no competing financial interest.

■ ACKNOWLEDGMENTS

We thank Dr. Bert H. Bakker (University of Amsterdam, The Netherlands) for providing the target compound and acknowledge financial support from the Fonds National Suisse de la Recherche Scientifique through project no. 200020-165890 and the University of Geneva.

■ REFERENCES

(1) *Hydrogen-Transfer Reactions*; Hynes, J. T., Klinman, J. P., Limbach, H.-H., Schowen, R. L., Eds.; Wiley-VCH: Weinheim, Germany, 2007.
(2) Chou, P.-T.; Solntsev, K. M. Photoinduced Proton Transfer in Chemistry and Biology. *J. Phys. Chem. B* **2015**, *119*, 2089−2089.
(3) Arnaut, L. G.; Formosinho, S. J. Excited-State Proton Transfer Reactions I. Fundamentals and Intermolecular Reactions. *J. Photochem. Photobiol., A* **1993**, *75*, 1−20.
(4) Tolbert, L. M.; Solntsev, K. M. Excited-State Proton Transfer: From Constrained Systems to "Super" Photoacids to Superfast Proton Transfer. *Acc. Chem. Res.* **2002**, *35*, 19−27.
(5) Agmon, N. Elementary Steps in Excited-State Proton Transfer. *J. Phys. Chem. A* **2005**, *109*, 13−35.
(6) Kumpulainen, T.; Lang, B.; Rosspeintner, A.; Vauthey, E. Ultrafast Elementary Photochemical Processes of Organic Molecules in Liquid Solution. *Chem. Rev.* **2017**, *117*, 10826−10939.
(7) Solntsev, K. M.; Huppert, D.; Agmon, N. Photochemistry of "Super"-Photoacids. Solvent Effects. *J. Phys. Chem. A* **1999**, *103*, 6984−6997.
(8) Spies, C.; Finkler, B.; Acar, N.; Jung, G. Solvatochromism of Pyranine-Derived Photoacids. *Phys. Chem. Chem. Phys.* **2013**, *15*, 19893−19905.
(9) Borgis, D.; Hynes, J. T. Curve Crossing Formulation for Proton Transfer Reactions in Solution. *J. Phys. Chem.* **1996**, *100*, 1118−1128.
(10) Kiefer, P. M.; Hynes, J. T. Adiabatic and Nonadiabatic Proton Transfer Rate Constants in Solution. *Solid State Ionics* **2004**, *168*, 219−224.
(11) Kiefer, P. M.; Hynes, J. T. *Hydrogen-Transfer Reactions*; Wiley-VCH: Weinheim, Germany, 2007; pp 303−348.
(12) Spry, D. B.; Goun, A.; Fayer, M. D. Deprotonation Dynamics and Stokes Shift of Pyranine (HPTS). *J. Phys. Chem. A* **2007**, *111*, 230−237.
(13) Pérez-Lustres, J. L.; Rodriguez-Prieto, F.; Mosquera, M.; Senyushkina, T. A.; Ernsting, N. P.; Kovalenko, S. A. Ultrafast Proton Transfer to Solvent: Molecularity and Intermediates from Solvation-

DOI: 10.1021/acs.jpclett.7b01956
J. Phys. Chem. Lett. 2017, 8, 4516−4521

and Diffusion-Controlled Regimes. *J. Am. Chem. Soc.* **2007**, *129*, 5408−5418.
(14) Veiga Gutiérrez, M.; Brenlla, A.; Carreira Blanco, C.; Fernández, B.; Kovalenko, S. A.; Rodríguez-Prieto, F.; Mosquera, M.; Lustres, J. L. P. Dissociation of a Strong Acid in Neat Solvents: Diffusion is Observed After Reversible Proton Ejection Inside the Solvent Shell. *J. Phys. Chem. B* **2013**, *117*, 14065−14078.
(15) Rumble, C. A.; Breffke, J.; Maroncelli, M. Solvation Dynamics and Proton Transfer in Diethylaminohydroxyflavone. *J. Phys. Chem. B* **2017**, *121*, 630−637.
(16) Weller, A. Fast Reactions of Excited Molecules. *Prog. React. Kinet.* **1961**, *1*, 187−214.
(17) Eigen, M. Proton Transfer, Acid-Base Catalysis, and Enzymatic Hydrolysis. Part I: Elementary Processes. *Angew. Chem., Int. Ed. Engl.* **1964**, *3*, 1−19.
(18) Leiderman, P.; Genosar, L.; Huppert, D. Excited-State Proton Transfer: Indication of Three Steps in the Dissociation and Recombination Process. *J. Phys. Chem. A* **2005**, *109*, 5965−5977.
(19) Brenlla, A.; Veiga Gutiérrez, M.; Ríos Rodríguez, M. C.; Rodríguez-Prieto, F.; Mosquera, M.; Pérez Lustres, J. L. Moderately Strong Photoacid Dissociates in Alcohols with High Transient Concentration of the Proton-Transfer Contact Pair. *J. Phys. Chem. Lett.* **2014**, *5*, 989−994.
(20) Sérgio Seixas de Melo, J.; Maçanita, A. L. Unveiling the Eigen-Weller Ion Pair from the Excited State Proton Transfer Kinetics of 3-Chloro-4-methyl-7-hydroxycoumarin. *J. Phys. Chem. B* **2015**, *119*, 2604−2610.
(21) Prayer, C.; Gustavsson, T.; Tran-Thi, T. H. What's new in the proton transfer reaction from pyranine to water? A femtosecond study of the proton transfer dynamics. *AIP Conf. Proc.* **1996**, *364*, 333−339.
(22) Tran-Thi, T. H.; Gustavsson, T.; Prayer, C.; Pommeret, S.; Hynes, J. T. Primary Ultrafast Events Preceding the Photoinduced Proton Transfer from Pyranine to Water. *Chem. Phys. Lett.* **2000**, *329*, 421−430.
(23) Spry, D. B.; Fayer, M. D. Observation of Slow Charge Redistribution Preceding Excited-State Proton Transfer. *J. Chem. Phys.* **2007**, *127*, 204501.
(24) Spry, D. B.; Fayer, M. D. Charge Redistribution and Photoacidity: Neutral Versus Cationic Photoacids. *J. Chem. Phys.* **2008**, *128*, 084508.
(25) Simkovitch, R.; Rozenman, G. G.; Huppert, D. A Fresh Look into the Time-Resolved Fluorescence of 8-Hydroxy-1,3,6-pyrenetrisulfonate with the use of the Fluorescence Up-Conversion Technique. *J. Photochem. Photobiol., A* **2017**, *344*, 15−27.
(26) Mohammed, O. F.; Dreyer, J.; Magnes, B.-Z.; Pines, E.; Nibbering, E. T. J. Solvent-Dependent Photoacidity State of Pyranine Monitored by Transient Mid-Infrared Spectroscopy. *ChemPhysChem* **2005**, *6*, 625−636.
(27) Liu, W.; Tang, L.; Oscar, B. G.; Wang, Y.; Chen, C.; Fang, C. Tracking Ultrafast Vibrational Cooling during Excited-State Proton Transfer Reaction with Anti-Stokes and Stokes Femtosecond Stimulated Raman Spectroscopy. *J. Phys. Chem. Lett.* **2017**, *8*, 997−1003.
(28) Kumpulainen, T.; Bakker, B. H.; Hilbers, M.; Brouwer, A. M. Synthesis and Spectroscopic Characterization of 1,8-Naphthalimide Derived "Super" Photoacids. *J. Phys. Chem. B* **2015**, *119*, 2515−2524.
(29) Gerecke, M.; Bierhance, G.; Gutmann, M.; Ernsting, N. P.; Rosspeintner, A. Femtosecond Broadband Fluorescence Upconversion Spectroscopy: Spectral Coverage Versus Efficiency. *Rev. Sci. Instrum.* **2016**, *87*, 053115.
(30) Rusch, P. F.; Lelieur, J. P. Analytical Moments of Skewed Gaussian Distribution Functions. *Anal. Chem.* **1973**, *45*, 1541−1543.
(31) Kumpulainen, T.; Rosspeintner, A.; Vauthey, E. Probe Dependence on Polar Solvation Dynamics from fs Broadband Fluorescence. *Phys. Chem. Chem. Phys.* **2017**, *19*, 8815−8825.
(32) Jagesar, D. C.; Hartl, F.; Buma, W. J.; Brouwer, A. M. Infrared Study of Intercomponent Interactions in a Switchable Hydrogen-Bonded Rotaxane. *Chem. - Eur. J.* **2008**, *14*, 1935−1946.
(33) Panman, M. R.; Bodis, P.; Shaw, D. J.; Bakker, B. H.; Newton, A. C.; Kay, E. R.; Leigh, D. A.; Buma, W. J.; Brouwer, A. M.; Woutersen, S. Time-Resolved Vibrational Spectroscopy of a Molecular Shuttle. *Phys. Chem. Chem. Phys.* **2012**, *14*, 1865−1875.
(34) Horng, M. L.; Gardecki, J. A.; Papazyan, A.; Maroncelli, M. Subpicosecond Measurements of Polar Solvation Dynamics − Coumarin-153 Revisited. *J. Phys. Chem.* **1995**, *99*, 17311−17337.
(35) According to the linear response theory assuming two displaced parabola, 50% of the dynamic Stokes shift originates from relaxation on the excited-state potential and another 50% originates from the displacement on the ground-state potential.
(36) Kumpulainen, T.; Brouwer, A. M. Excited-State Proton Transfer and Ion Pair Formation in a Cinchona Organocatalyst. *Phys. Chem. Chem. Phys.* **2012**, *14*, 13019−13026.
(37) Simkovitch, R.; Akulov, K.; Shomer, S.; Roth, M. E.; Shabat, D.; Schwartz, T.; Huppert, D. Comprehensive Study of Ultrafast Excited-State Proton Transfer in Water and D_2O Providing the Missing $RO^-\cdots H^+$ Ion-Pair Fingerprint. *J. Phys. Chem. A* **2014**, *118*, 4425−4443.
(38) Kumpulainen, T.; Bakker, B. H.; Brouwer, A. M. Complexes of a Naphthalimide Photoacid with Organic Bases, and Their Excited-State Dynamics in Polar Aprotic Organic Solvents. *Phys. Chem. Chem. Phys.* **2015**, *17*, 20715−20724.

DOI: 10.1021/acs.jpclett.7b01956
J. Phys. Chem. Lett. 2017, 8, 4516−4521